# Genome-Wide Assessment in *Escherichia coli* Reveals Time-Dependent Nanotoxicity Paradigms

Vincent C. Reyes,[†] Minghua Li,[†,‡,||] Eric M. V. Hoek,[†,‡] Shaily Mahendra,[†] and Robert Damoiseaux[‡,§,⊥,*]

[†]Department of Civil & Environmental Engineering, [‡]California NanoSystems Institute, [§]Molecular Screening Shared Resource, and [⊥]Center for Environmental Implications of Nanotechnonolgy, University of California, Los Angeles, California 90095, United States and [||]Nalco Company, Naperville, Illinois 60563, United States

ABSTRACT The use of engineered nanomaterials (eNM) in consumer and industrial products is increasing exponentially. Our ability to rapidly assess their potential effects on human and environmental health is limited by our understanding of nanomediated toxicity. High-throughput screening (HTS) enables the investigation of nanomediated toxicity on a genome-wide level, thus uncovering their novel mechanisms and paradigms. Herein, we investigate the toxicity of zinc-containing nanomaterials (Zn-eNMs) using a time-resolved HTS methodology in an arrayed *Escherichia coli* genome-wide knockout (KO) library. The library was

KO Clone Library Exposed to NMs — Differential Growth Measured — Time Dependant Sensitivity Observed

screened against nanoscale zerovalent zinc (nZn), nanoscale zinc oxide (nZnO), and zinc chloride (ZnCl₂) salt as reference. Through sequential screening over 24 h, our method identified 173 sensitive clones from diverse biological pathways, which fell into two general groups: early and late responders. The overlap between these groups was small. Our results suggest that bacterial toxicity mechanisms change from pathways related to general metabolic function, transport, signaling, and metal ion homeostasis to membrane synthesis pathways over time. While all zinc sources shared pathways relating to membrane damage and metal ion homeostasis, Zn-eNMs and ZnCl₂ displayed differences in their sensitivity profiles. For example, ZnCl₂ and nZnO elicited unique responses in pathways related to two-component signaling and monosaccharide biosynthesis, respectively. Single isolated measurements, such as MIC or IC_{50}, are inadequate, and time-resolved approaches utilizing genome-wide assays are therefore needed to capture this crucial dimension and illuminate the dynamic interplay at the nano-bio interface.
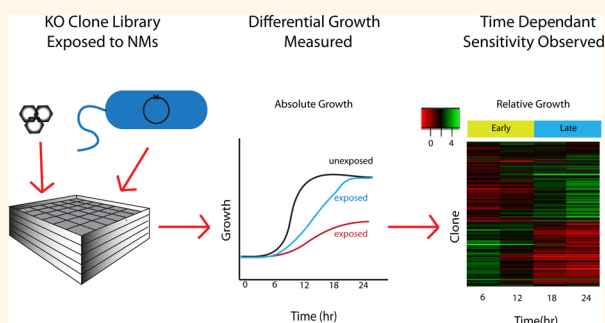
KEYWORDS: nanomaterial · nanoparticle · nanotoxicity · zinc · zinc oxide · zinc chloride · high-throughput screening · Keio knockout library · *E. coli* · cytotoxicity · toxicity mechanism

Within the burgeoning field of engineered nanomaterials (eNM), zinc-containing nanomaterials (Zn-eNMs), such as nanoscale zerovalent zinc (nZn) and zinc oxide (nZnO), have emerged among the most widely used (http://www.nanotechproject.org) and toxic.[1−4] Zn-eNMs are currently used in consumer and industrial products such as cosmetics, paints, plastics, tires, and sunscreens and are being developed for water disinfection and chemotherapeutic applications.[5−7] Comprehensive identification and understanding of Zn-eNM's toxicity paradigms and mechanisms is crucial for developing regulations for safer eNMs and protecting ecological and human health.[8]

Interestingly, while researchers have observed toxic responses in organisms at every trophic level—including mammalian cells, algae, bacteria, plants, crustacean, and fish—the mechanisms of Zn-eNM toxicity remain unresolved.[2,5,6,10−13] Despite exploration of various toxicity mechanisms, researchers remain divided on whether toxicity results primarily from the release of free Zn^{2+} ions or unique Zn-eNM-specific properties. For example, in eukaryotic cells, researchers have observed DNA damage, ROS generation, and membrane leakage and depolarization after Zn-eNM exposure.[1,14] George and co-workers showed the importance of ions by slowing the Zn^{2+} release rate from Zn-eNMs, which resulted in reduced toxicity in lung epithelial and macrophage cells.[15] In contrast, Lin and co-workers found that limited dissolution of Zn^{2+} in the culture media did not allow ions to contribute to

cytotoxicity in lung epithelial cells.[16] Similar discrepancies in toxicity mechanisms have been observed in prokaryotes. Various studies observed that free Zn^{2+} in solution determined toxicity for Zn-eNMs.[17] For example, Li and co-workers showed that media components that bound to the free zinc ions substantially reduced their toxicity toward *Escherichia coli* (*E. coli*) cells.[10] However, different studies of *E. coli* suggest that the attachment of Zn-eNMs or their aggregates was responsible for toxicity, while others observed leakages in the cell membrane after exposure to nZnO but not from the respective salt, $ZnCl_2$.[2,11,12] The observed discrepancies highlight the need for a comprehensive assessment of toxicity mechanisms.

Genome-wide high-throughput methodologies offer a solution to this problem by enabling the examination of all potential mechanisms in parallel.[18] In contrast, traditional toxicity assays examine a single toxicity paradigm at a time and require *a priori* knowledge of the target. Genome-wide approaches, such as microarrays have been employed to track the response of thousands of genes and pathways to Zn-eNMs and other eNMs.[19,20] However, microarrays suffer from the biases of DNA/RNA extraction and amplification, do not reflect changes in translational and post-translational modifications, and are unable to profile dead cells in which degradation of mRNAs is prominent.[22] Furthermore, chip-based approaches typically only reflect a single time point due to cost and labor constraints.[21,22] Furthermore, the resulting single time point measurements ignore temporal changes in the eNMs stemming from aggregation, dissolution, precipitation, eNM aging, or acquisition of coatings which affect their interactions with cells.[23,24] Another potential approach is the use of a collection of reporter gene constructs utilizing green fluorescent protein (GFP) fusions in *E. coli* to track differential gene expression in response to eNMs in a time-resolved manner.[25] This methodology is limited as it only reports on a selected subset of genes and is unable to measure biological responses under lethal conditions. Furthermore, the selection of promoters for reporter genes assumes some prior knowledge of the toxicity mechanisms. In conclusion, complete toxicological assessments of eNMs must utilize time-resolved genome-wide high-throughput methodologies.

Here, we address the limitations of current approaches by employing a time-resolved high-throughput screening (HTS) methodology using an arrayed genome-wide *E. coli* knockout (KO) library to assess the Zn-eNM stress response. Our approach does not require *a priori* knowledge of toxicity mechanisms, as the library comprises roughly 4000 clones allowing for nearly 90% of the *E. coli* genome to be scanned.[26] Through this methodology, we explored the biological responses of the model organism, *E. coli*, to Zn-eNMs and salts on a genome-wide scale, identified sensitive pathways, and examined the changes in these mechanisms over time. Our results indicate that traditional single time point measurements will continue to fail to recognize these changes in toxicity mechanisms. Our genome-wide time-resolved methodology, however, has the potential to provide a comprehensive assessment of eNM toxicity, which is crucial for the correct assessment of nanotoxicity and safe design of eNMs, and may become the standard for eNM safety profiling.

RESULTS

Overall Methodology. A time-resolved HTS methodology using the Keio *E. coli* genome-wide KO clone library was developed to examine the bacterial toxicity of Zn-eNMs (nanoscale zerovalent zinc (nZn), nanoscale zinc oxide (nZnO), and zinc chloride ($ZnCl_2$) salt for reference). As each clone lacks a single gene, the sensitivity of multiple clones in a given pathway, cellular compartment, or cellular process to a zinc source suggests a particular toxicity paradigm or mechanism. This approach is in sharp contrast to conventional approaches that typically screen for individual targets. Furthermore, where conventional screens rely on single time point measurements, our methodology is based on screening across multiple time points and concentrations. In short, our approach comprised two stages, an initial KO screen to identify sensitive clones (Figure 1A) and then secondary screening to determine IC_{50} values for each clone to identify absolute differences among clones (Figure 1B) at two time points. Figure 1 summarizes the approach and results of our methodology, and further details are elaborated below and in the Materials and Methods section.

Physical−Chemical Properties. Both Zn-eNMS in powder form exhibited large variation in size. The average primary particle size reported by the manufacturer for nZn and nZnO was 92.5 and 10.0 nm, respectively. In the dry powdered form, both appeared aggregated (Figure 2A). On the basis of FESEM observations, the morphologies and sizes of both nanoparticles did not vary significantly after suspending in Luria−Bertani (LB) broth media (∼100−160 nm). Observed particles consisted of both insoluble Zn-eNMs and particles formed by the reprecipitation of dissolved Zn^{2+} with counterions such as PO_4^{3-} in LB media. Relative to Zn-eNMs, precipitates formed by excess $ZnCl_2$ salts were an order of magnitude smaller (18 ± 4 nm).

During the 24 h incubation in LB, the zeta-potential (∼20 mV) of nZnO remained constant in LB, while the zeta-potential of nZn decreased from −27.6 to −17.5 mV nearing the range of nZnO (Table S1 in Supporting Information). This suggests that an oxide layer formed on the particles in solution. The aggregate size of the particles as measured by hydrodynamic diameter, however, increased initially but remained consistent after 6 h of incubation (Table S1). Generally,
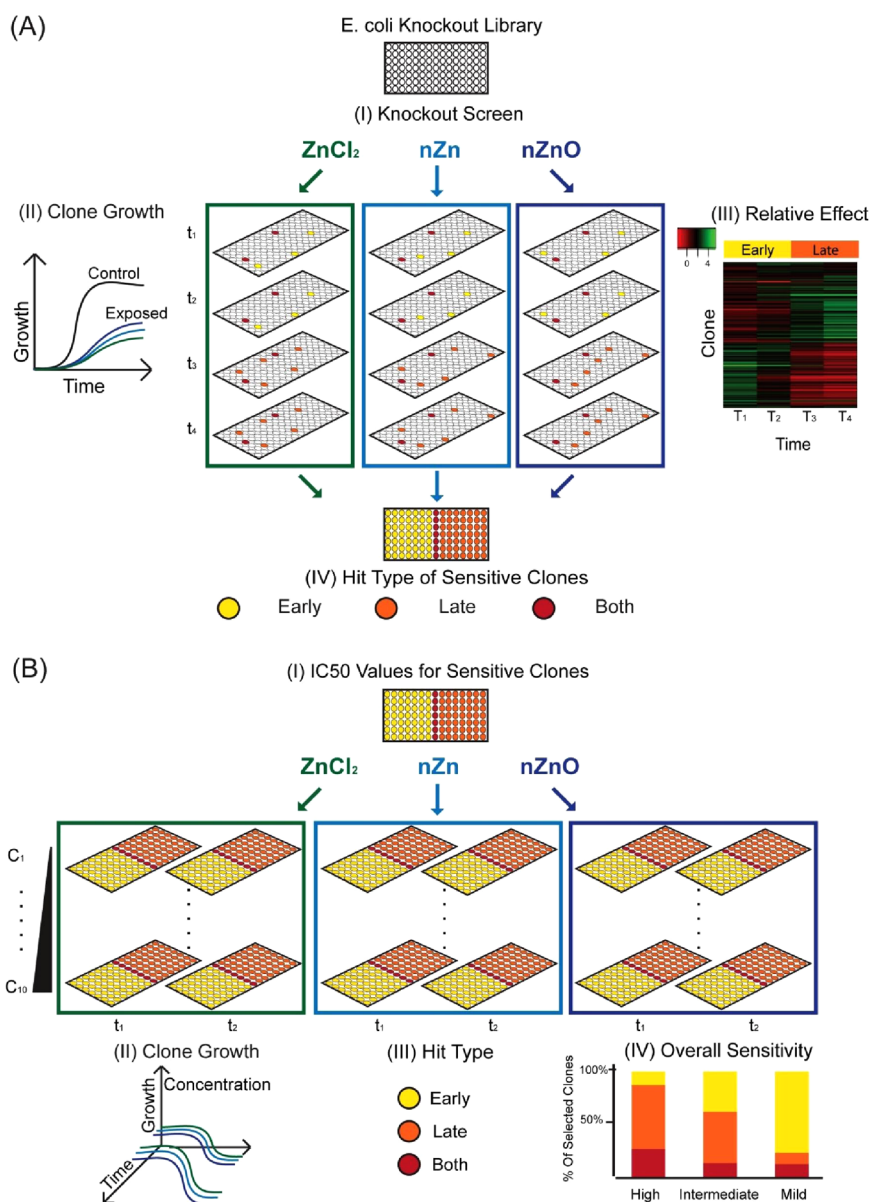
Figure 1. Overview of experimental procedures and results. A high-throughput screening (HTS) methodology using an *E. coli* genome-wide knockout (KO) clone library was developed to examine bacterial toxicity of zinc-containing eNMs (nanoscale zerovalent zinc (nZn), nanoscale zinc oxide (nZnO), and zinc chloride (ZnCl$_2$) salt for reference). As each clone lacks a single gene, the sensitivity of a group of related clones to a zinc source suggests a particular toxicity mechanism. This approach comprised two components: (A) initial KO screen to identify sensitive clones and (B) determining IC$_{50}$ values for each to identify absolute differences among clones. In the KO screen (A), clone growth (OD$_{600nm}$) after exposure to a single wild-type IC$_{50}$ concentration of each zinc source (nZn, nZnO, and the control, ZnCl$_2$) was monitored over 24 h ($t = 6, 12, 18$, and 24 h) (I,II). The ratio of the log$_2$ OD$_{600nm}$ values of the exposed clones to the unexposed clones was used to normalize among clones. Next, a Z-score methodology controlling experimental variation identified 173 clones displaying statistically significant growth reduction (hits). Hierarchal cluster analysis (HCA) in combination with heat maps was used to identify trends among sensitive clones (III). In addition to zinc source specific differences, many clones were only hits at early (6−12 h) or late (18−24 h) times. Few were hits at both times, and hits from each time point represented different biological categories. These sensitive clones were isolated from the library and subjected to further characterization (IV). Clone-specific IC$_{50}$ concentrations were determined at an early (8 h) and late (22 h) time point (B). In contrast to the relative metrics used in the initial screening, the absolute metric of IC$_{50}$ was determined for comparison. Clones were exposed to 10 concentrations around the IC$_{50}$ of each zinc source (three 2-fold dilutions above and seven 2-fold dilutions below), and growth was measured at both time points (I,II). Clones exhibited high, intermediate, and mild sensitivity (IC$_{50}$), which reflected their time-dependent sensitivity. High sensitivity clones displayed low IC$_{50}$ values at both time periods, while intermediate and mild sensitivity clones showed varying degrees of recovery (high IC$_{50}$). Overall, clones displaying high sensitivity were more likely to have been identified as late hits in the KO screen, while mild sensitivity clones were more likely to be detected as early hits (IV). These results suggest that eNM toxicity changes with time and that single time point measurements cannot capture this dimension.

nZn aggregate sizes were 2× those of nZnO. While their hydrodynamic diameter changed slightly over 24 h, the dissolved Zn^{2+} ion concentrations were similar throughout all three zinc solutions with roughly

(A) Aggregate Particle Size
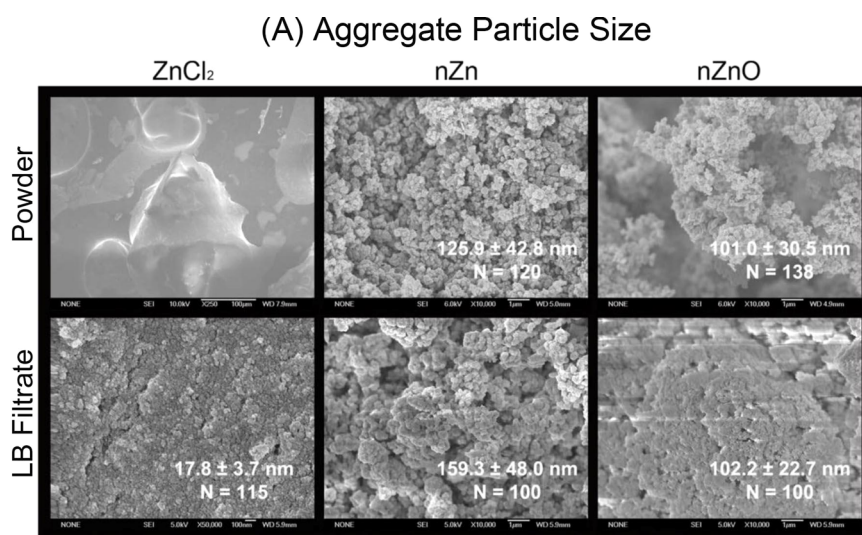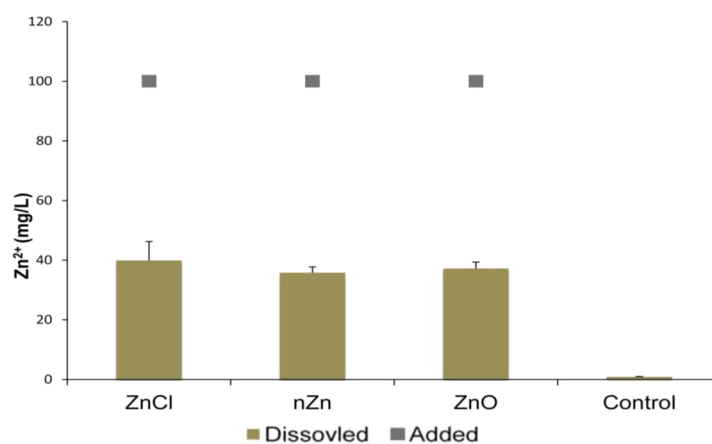

(B) Zinc Concentration

Figure 2. Aggregate particle size of powders and resulting filtrate after 24 h incubation in LB visualized by FESEM (A) and the dissolved Zn^{2+} concentration after 24 h incubation in LB media (B). The morphology of both NMs did not vary significantly after suspending in LB media, and aggregate sizes in the filtrate remained in the same range as the powder. $ZnCl_2$ aggregates were an order of magnitude smaller than NM aggregates. Relative to ion concentrations, Zn^{2+} ions released from Zn-eNMs and $ZnCl_2$ in LB as measured by ICP-OES were nearly equal with roughly 40% of the added concentration for each.

40% of the total added Zn^{2+} present in the media as free ions (Figure 2B). The concentration of free Zn^{2+} in LB without added zinc was 0.86 ± 0.09 mg/L.

The chemical compositions of Zn-eNMs and salts before and after suspension in LB media are summarized in Figure S1. The oxygen peak appeared in EDAX analysis for pure nZn powder, implying oxidation of nZn powder during storage. As the X-ray probe does not completely penetrate the sample, our results suggest only surface layer oxidation or the formation of $Zn(OH)_2$. Furthermore, the Zn/O molar ratio for nZn was 1:0.93, which was near the Zn/O ratio observed for nZnO (1:1.08). As the formation of an oxide layer is likely under an aerobic environment, this reflects exposure parameters in various environments where NMs may be released. When exposed to LB, significant amounts of phosphorus appeared in the solids collected from nZn and nZnO suspensions in LB media.

The oxygen content (with respect to Zn) in those samples showed appreciable increases, as well. This implies the presence of $Zn_3(PO_4)_2$, which has a solubility product of $K_{sp} = 9.0 \times 10^{-33}$ among other species.[10] For $ZnCl_2$, although the salt has high solubility in water, other counterions present in the media, such as OH^- and PO_4^{3-}, can also form precipitates with Zn^{2+}. From the EDAX result, the Zn/P/O ratio was 1:0.50:3.39, which is close to the atomic ratio of $Zn_3(PO_4)_2$ (i.e., 1:0.67:2.67), suggesting that $Zn_3(PO_4)_2$ was also the dominant precipitated species. The ratio is not exact as the precipitation was expected to be a mixture of different Zn salts; therefore, it is expected to only have a rough match.

Time-Resolved Wild-Type IC_{50}. Exposing the wild-type (wt) strain to a dilution series of Zn-eNMs and salts (0.2–500 mg/L as total Zn^{2+} added) revealed that $ZnCl_2$ was the most toxic followed by nZnO, then

nZn (Table S2). Among all three zinc sources, there was an overall increase in IC_{50} values throughout the 24 h period. The decrease in toxicity varied between zinc sources. The IC_{50} values for $ZnCl_2$, for example, increased nearly 75% (40.7 mg/L [6 h]—71.07 mg/L [24 h]), while nZn IC_{50} values increased only by about 36% (96.41 mg/L [6 h]—131.6 mg/L [24 h]).

KO Library Screen. The Keio *E. coli* KO library was exposed to the IC_{50} concentration of each zinc source obtained from the wt data (Table S2), and growth inhibition (transmittance: OD_{600nm}) was assessed over a 24 h period. Growth inhibition was assessed every 6 h to capture to the lag, exponential, and stationary growth phases. As each clone has a different growth profile, we ran a copy of the library with no added zinc in parallel for reference. For data mining, the ratio of the $\log_2$ transmittance values of the exposed clones to the unexposed clones was formed, and a robust Z-score method was employed to identify statistically sensitive clones and control for differences among clones and run-to-run and plate-to-plate variation.[27] Further details can be found in the Materials and Methods section and Figure 1, which summarizes these methods and results of the KO library screening (1A) and IC_{50} values of sensitive clones (1B). Of the 3985 clones screened, 173 clones exhibited an increased sensitivity to $ZnCl_2$, nZn, or nZnO at any of the four time points surveyed resulting in a cumulative hit rate of 4.3% (for details, see Tables S3 and S4: (A) Z-score). The heat map in Figure 3A summarizes the Z-scores of the selected clones, in which the green spectra colors indicate positive Z-scores (more sensitive) and Z-scores greater than 2.5 were classified as hits.[28] Using hierarchical cluster analysis (HCA), we observed a distinct dichotomy between early and late responding clones which conventional single time point approaches would have missed. HCA grouped the earlier 6 and 12 h time points together and the later 18 and 24 h time points together (Figure 3A,B). This resulted in 106 "early" and 91 "late" hits with only 24 hits shared between time periods (Figure 3B and Table S4 (B): time).

$ZnCl_2$ had the most pronounced effect on the clones as it elicited 112 total hits, with 70 unique hits (62%) that were not detected by either Zn-eNM (Figure 3C and Table S4 (C): source). In contrast, only 17 of 77 total (22%) nZn sensitive clones and 19 of 81 total (23%) nZnO sensitive clones were unique for either Zn-eNM. Thirty clones were shared hits by all three zinc sources, while the remaining 37 clones were shared hits for both Zn-eNMs (25), $ZnCl_2$ and nZn (7), or $ZnCl_2$ and nZnO (5). Furthermore, in addition to sharing multiple hits between Zn-eNMs (71% for nZn and 68% nZnO), the Z-scores for both were clustered together at each time point (Figure 3A). $ZnCl_2$, in contrast, formed its own cluster at the late time periods (18 and 24 h). This suggests that the toxicological profiles of the
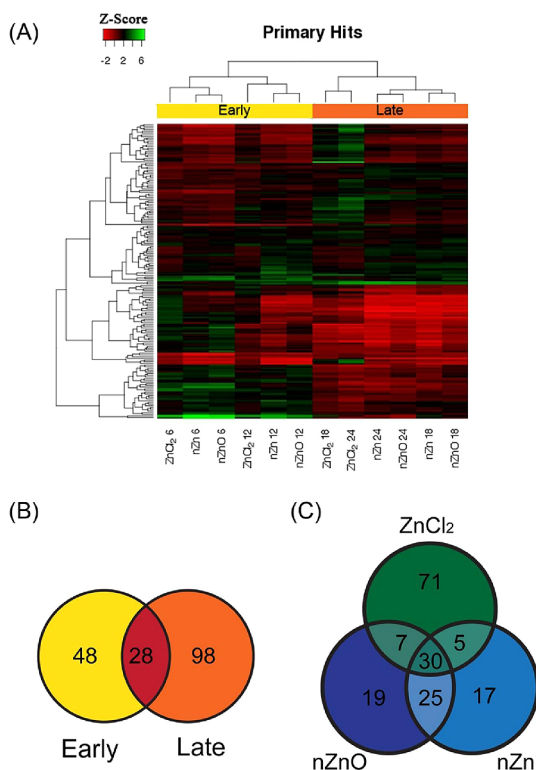

Figure 3. Z-scores for the 173 sensitive clones detected after exposure to $ZnCl_2$, nZn, and nZnO at four time points (6, 12, 18, and 24 h) (A) and distribution between categories (B,C). For the heat map (A), green spectrum colors indicate positive Z-scores (more sensitive) while red spectrum colors indicate negative Z-scores (less sensitive). Hierarchical clustering analysis was used to determine similarities among Z-scores. In general, clustering suggests that Z-scores varied across time and among zinc sources. Tight clustering was observed between early hits (6 and 12 h) and late hits (18 and 24 h), which supports a temporal dichotomy in responses to zinc. KO library screening hit distribution varied for hits across time (B) and hits across source (C).

Zn-eNMs were more closely related than $ZnCl_2$ and suggests nanorelated toxicity paradigms.

In order to enable further data interpretation and the detection of nanorelated toxicity pathways, the Database for Annotation, Visualization and Integrated Discovery (DAVID) v6.7's functional annotation clustering algorithm was used to determine the over-representation of annotation terms from the clones detected relative to their presence in the *E. coli* genome. The results are shown in Figure 4: functional annotation clustering of the entire sensitive clone list resulted in the enrichment of eight functional clusters, representing five general biological categories, metal homeostasis (metal ion transport and metal ion biding), membrane-related (lipopolysaccharide biosynthesis and cell membrane structure), transport (ABC transporters), central metabolic reactions (monosaccharide metabolism), and regulation and signaling (transcription regulation and two-component signaling) (for details, see Table S4: (D) functional clusters, and Table S5). For the gene list as a whole, all clusters were significantly enriched based on a
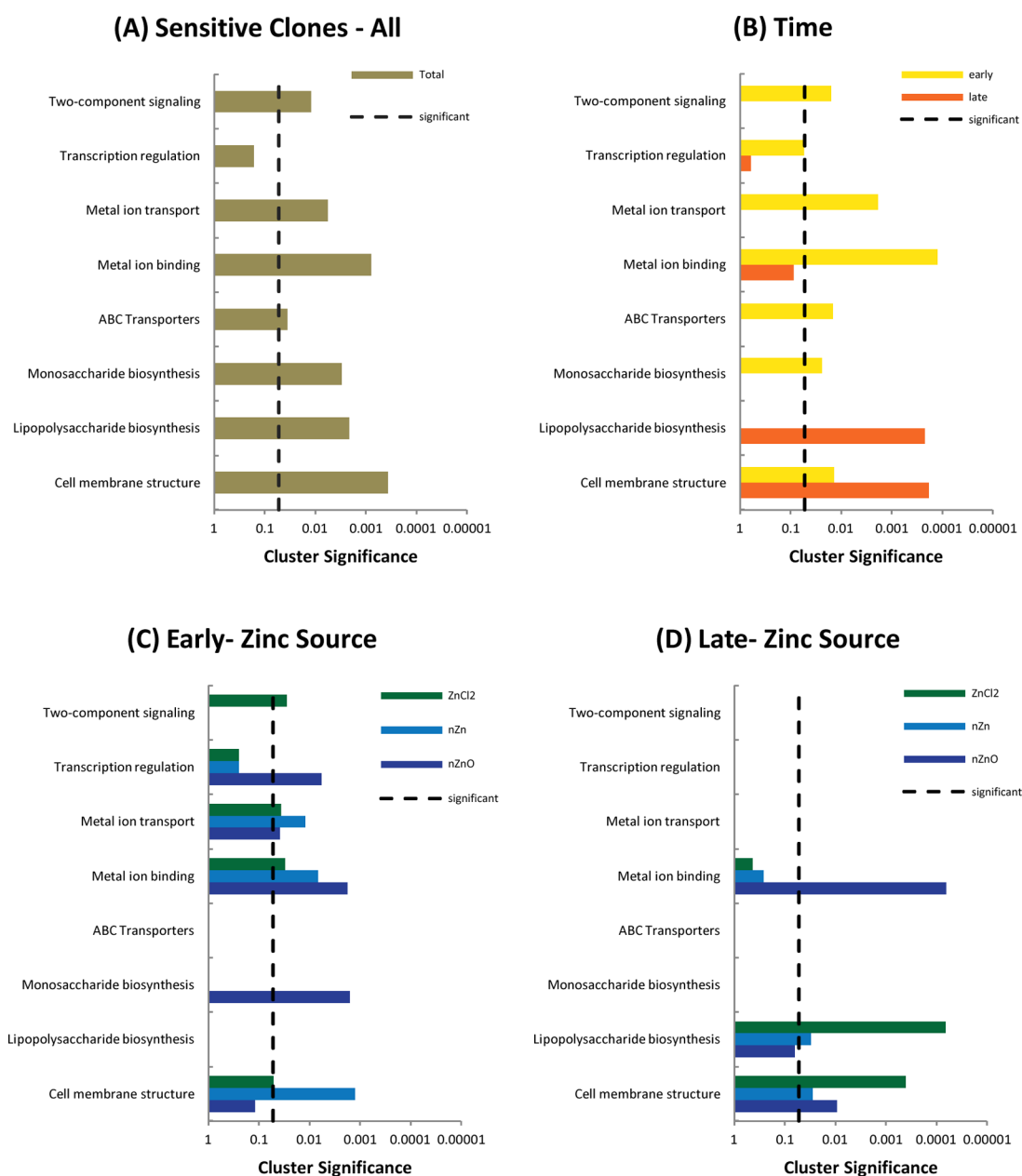
Figure 4. Functional clustering analysis for sensitive clones in KO Library screening. Cluster significance shows the over-representation of related annotation terms of the sensitive clones relative to their presence in the *E. coli* genome. Enrichment cluster analysis was performed for hits in the following categories: (A) sensitive clones, all; (B) time; (C) early, source; and (D) late, source. In total, the sensitive strains enriched for eight clusters spanning five general biological categories: (1) regulation and signaling (two-component signaling and transcription regulation), (2) metal homeostasis (metal ion binding and metal ion transport), (3) transport (ABC transporters), (4) central metabolic reaction (monosaccharide metabolism), and (6) membrane-related (lipopolysaccharide biosynthesis and cell membrane structure). Temporally, early hits affected general metabolism, transport, transcription and regulation, and metal ion binding and transport, while later hits enriched for genes related to membrane generation and structure. Relative to zinc source, all metals enriched for clusters related to metal ion binding and transport at early time points and membrane generation and structure at later time points.

combined *p* value of 0.05 with the exception of transcription regulation (see Figure 4A), which appeared enriched to a lesser extent. Combined *p* values were calculated as the geometric mean of the enrichment *p* values for each annotation term associated with the genes in each cluster.[29] It is important to note that the size of the functional clusters was not equal for all clusters. For example, metal ion binding and cell membrane

structure contained 29 and 27 genes, respectively, while the monosaccharide metabolism cluster, which had the fewest members, only had eight genes with the fewest members (Table S4: (D) functional clusters).

Next, we broke the data into early and late time points and re-analyzed for enrichment in functional clusters (see Figure 4B). Specifically, clusters relating to two-component signaling, metal ion transport and

(A) Heat maps of IC$_{50}$ Values

ZnCl$_2$ IC$_{50}$ values

nZn IC$_{50}$ values

nZnO IC$_{50}$ values
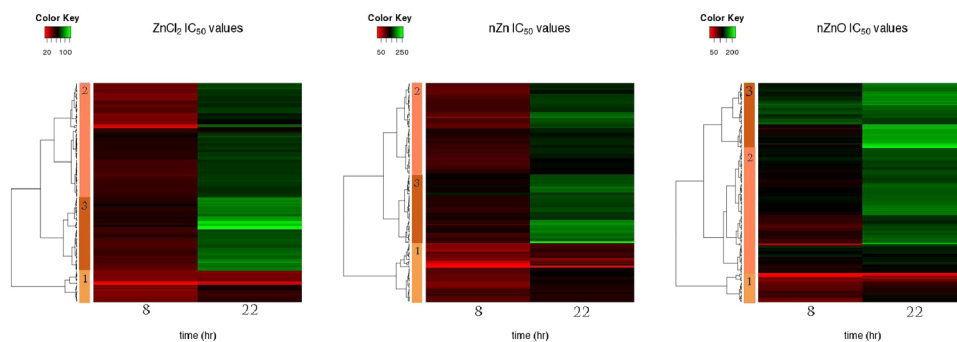
(B) Clone IC$_{50}$ (mg/L) mean values ± std dev

	8 hrs			22 hr		
	ZnCl$_2$	nZn	nZnO	ZnC$_{l2}$	nZn	nZnO
Overall sensitivity	50.64 ± 9.36	103.01 ± 21.71	111.92 ± 23.52	78.10 ± 15.97	148.92 ± 30.46	144.97 ± 30.00
High sensitivity	38.35 ± 8.14	80.03 ± 23.25	72.38 ± 24.25	49.47 ± 12.22	112.07 ± 23.90	92.270 ± 28.82
Intermediate sensitivity	50.89 ± 8.85	104.3 ± 10.89	111.6 ± 13.83	76.64 ± 4.75	152.46 ± 13.63	143.89 ± 14.91
Mild sensitivity	55.53 ± 4.83	121.2 ± 10.04	129.8 ± 14.88	92.71 ± 9.75	176.16 ± 17.38	170.31 ± 18.86

Figure 5. Time-resolved IC$_{50}$ values: heat maps of sensitive clones show differential shifts in IC$_{50}$ values over time (A), and the chart displays the mean IC$_{50}$ values of each category (B). Relative to the heat maps, green spectrum colors represent high values and red spectrum colors represent low values. Hierarchal cluster analysis on each set of IC$_{50}$ values divided clones into three categories: (1) high sensitivity, (2) intermediate sensitivity, and (3) mild sensitivity. High sensitivity clones had low IC$_{50}$ values at both time points, while mild sensitivity clones had initially low IC$_{50}$ values at 8 h, but increased to higher values at 22 h. Intermediately sensitive clones were between these two conditions. The clusters generally agreed among sources. Differences in the IC$_{50}$ values of each sensitivity category are reflected by the mean IC$_{50}$ values, which increase with time (B). ZnCl$_2$ was more toxic than either Zn-eNM.

binding, ABC transport, and monosaccharide biosynthesis were more enriched during earlier time points, while clusters related to lipopolysaccharide biosynthesis and cell membrane structure were more enriched at later time points (Table S5: (D) functional clusters). Moreover, when we subdivided the data further for early and late time points and by zinc source (Figure 4C, D), much of the enrichment was retained. Most importantly, subdivision into nanoscale and bulk materials leads to the appearance of functional clusters specific for nanoscale or bulk materials both for early and late time points. Of the clusters for the early time points, both bulk and nanomaterial showed more enrichment of clusters related to metal homeostasis (metal ion transport and binding) and transcription regulation (Figure 4C). Only ZnCl$_2$ enriched for the gene cluster related to two-component signaling, while nZnO enriched for the cluster related to monosaccharide biosynthesis. This cluster is missing in the late time points and would have been missed using conventional single-point assays. The same goes to some extent for nZn and the cell membrane structure cluster, albeit it is somewhat retained for later time points. Interestingly, all three zinc sources displayed enrichment for clusters related to membrane structure (lipopolysaccharide biosynthesis and cell membrane structure) during the late time points (Figure 4D), but only nZnO shows a highly enriched

cluster for metal ion binding. In short, most of the enrichment of functional clusters is time-dependent irrespectively of eNM or bulk material, and functional clusters specific for both eNM and bulk material can be found.

IC$_{50}$ Values of Sensitive Clones. The clones which we determined to be sensitive to bulk or nanoforms of Zn were further characterized by IC$_{50}$ measurements at an early (8 h) and late (22 h) time point for each zinc source to investigate the observed trends further (see Figure 5 for results). The methodology and subsequent characterization of clones is summarized in Figure 1B, and further details can be found in the Materials and Methods section. In contrast to the relative differences in sensitivities observed in the KO library screen, IC$_{50}$ values represent an absolute metric for comparison of the fitness of a given KO clone. Overall, the IC$_{50}$ values for the selected clones exhibited a time-dependent increase which was similar to those observed in the wt (Figure 5 and Table S2) with ZnCl$_2$ exposure resulting in the lowest IC$_{50}$ values for both the wt and sensitive clones. It is not surprising that the wt and clones do not match up exactly as the growth pattern in a given KO clone results in part from growth compensation in the absence of a particular gene which is different from wt growth. Overall, the clones *ZntA* and *ZntR* displayed consistently the lowest IC$_{50}$ values (Table S4: (F) IC$_{50}$). Across all three zinc sources, their IC$_{50}$ values remained

at $\sim$10−20 mg/L at both time points, which is $\sim$4−7-fold lower than the overall averages.

IC$_{50}$ values repeat the dichotomy observed in the KO screen between early and late hits as some clones had initially low IC$_{50}$ values, but recovered, while other clones maintained low IC$_{50}$ values throughout (Figure 5A). HCA was used on each zinc source to divide the clones into three subgroups: high, intermediate, and mild sensitivity. High sensitivity clones had the lowest IC$_{50}$ values at both time points, while mild sensitivity clones had initially low IC$_{50}$ values at 8 h, but increased to high values at 24 h; that is, the clones recovered to normal growth, which was also observed during primary screening. Intermediately sensitive clones were between these two extremes. Mean values of each category across time points highlight these results (Figure 5B). To characterize overall sensitivity, clones were grouped into the category in which it was classified the most across all three metals. Generally, clones fell into the same category across zinc sources, and discrepancies varied by one level of sensitivity. Only four clones (*gpt, ybdD, yijP,* and *yebA*) spanned more than one level of sensitivity, and these outliers together did not represent any collective functional category (Table S4: (F) IC$_{50}$). This resulted in 26 high, 94 intermediate, and 53 mild sensitivity clones. Interestingly, those clones classified as late hits or shared hits between time points were more likely to be classified as high sensitivity clones, while those classified as early hits were more likely to be detected as mild sensitivity clones (Figure 6A). For example, in overall sensitivity, nearly 93% of the high sensitivity clones were late or shared hits, while 81% of the mild sensitivity clones were early hits. This trend was evident in the overall classifications of sensitivities and for the sensitivities derived from exposure to each zinc source. This suggests that highly sensitive hits can be detected at both time periods, while mild hits are lost at later time periods.

Functional annotation clustering of clones at each level of sensitivity revealed distinct categories of enrichment and reflects clusters identified by the early and late hits (Figure 6B). Mild sensitivity clones had more enrichment in categories related to two-component signaling and ABC transporters, while high and intermediate sensitivity clones enriched for lipopolysaccharide biosynthesis and cell membrane structure. Categories related to metal ion binding and transport were present at all three levels of sensitivities. This suggests that toxicity mechanisms as reflected by the different clusters may be evident at different times, depending on when toxicity is assessed.

DISCUSSION

Engineered nanomaterials are subject to physical processes such as aggregation, dissolution, and precipitation of dissolved ions that occur over time.[23]
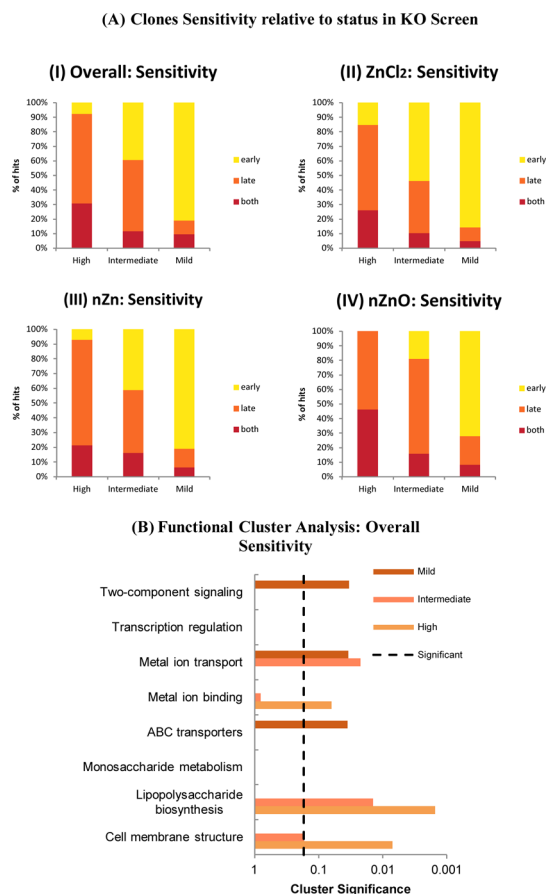

Figure 6. Clone sensitivity for IC$_{50}$ clustering relative to their status from primary screening for (I) overall and separated by source: (II) ZnCl$_2$, (III) nZn, (IV) nZnO (A). Regardless of source, those hits which were categorized as late hits are more likely to display high sensitivity, while those detected as early hits are more likely to display mild sensitivity. As clusters agreed among sources, functional clustering analysis was performed for the clones overall sensitivity (B). Cluster significance displays the overrepresentation of related annotation terms of the sensitive clones relative to their presence in the *E. coli* genome. All three levels of sensitivities share categories related to metal ion binding and transport. Clones with mild sensitivity had more enrichment in clusters related to signaling and transport, while high sensitivity clones and intermediate sensitivity clones enriched more for membrane-related clusters.

Similarly, biological responses such as adhesion, absorption, and transformation of a foreign material also vary with time.[30] As a single time point measurement cannot capture these changes, only time-resolved methodologies can incorporate the temporal differences in chemistry and biology to reliably assess the dynamic interactions of eNMs with organisms. While some current approaches have attempted to incorporate the temporal dimension, a comprehensive and unbiased study has not been conducted to date due to cost and technological limitations. Here, we presented a genome-wide time-resolved HTS methodology, which we applied toward the identification of toxicity pathways in *E. coli* using widely available nZn and nZnO as model eNMs and ZnCl$_2$ as a reference.

We evaluated the sensitivities in an *E. coli* genome-wide KO library over a 24 h period and identified 173 clones sensitive to zinc eNMs and/or $ZnCl_2$.

Importantly, these 173 clones were not equally sensitive over the entire 24 h nor were they equally sensitive to all zinc sources at each time point. We found a pronounced dichotomy between early and late time points with only a small portion of the clones being shared between early and late time points. Many of the clones displaying early sensitivity recovered and would have not been detected by conventional end-point assays such as IC_{50} values, which miss a substantial portion of the toxicity response. More importantly, the clones sensitive at early time points showed markedly different enrichment of biological pathways (*i.e.*, clusters) from late responders. Clones related to signaling and regulation (two-component signaling and transcription regulation), transport (ABC transport), and central metabolic reactions (monosaccharide biosynthesis) were more enriched at early time points (8 and 12 h), while membrane-related clusters (lipopolysaccharide biosynthesis and cell membrane structures) were more enriched at later times (12 and 24 h). Clones relating to metal homeostasis were detected at both time points, but they experienced greater enrichment earlier. As a result, end-point assays have limited usefulness for the safety assessment of materials, as they do not allow for building models on a complete data sets.

Even more significantly, this time-dependent behavior was consistent for the entirety of the sensitive clones. Time dependence was well pronounced when subdividing the clones into bulk and nanomaterial reflecting their specific toxicity paradigms. For example, during early time points, nZnO showed enrichment in monosaccharide biosynthesis and transcription regulation clusters while nZn showed enrichment in cell membrane structure clusters. Interestingly, nZnO showed enrichment at late time points for metal ion binding, while $ZnCl_2$ and nZn did not enrich in this cluster at this time point. The differences in cluster enrichment point to different toxicity pathways and paradigms, which are dependent on the growth phase of the bacterial culture. Specifically, the enrichment of clones related to general metabolism (monosaccharide biosynthesis) by nZnO and two-component signaling by $ZnCl_2$ during early time points may reflect the changing constraints found at different bacterial growth phases. Measurements taken at early time points (6 and 12 h) reflect *E. coli* cells in or near exponential growth. Clones related to the cluster monosaccharide biosynthesis participate in important processes such as glycolysis and the pentose phosphate pathway, which are essential for energy generation during exponential growth. Similarly, of early responding clones in the cluster two-component signaling, all except one (11 of 12) are necessary for shifts in metabolism and utilization of specific compounds (carbon utility: *arcB*, *creC*, *dcuS*, *frwB*, *pgm*, *pfkB*, *ptsI*, and *ptsP*; nitrogen: *glnL*; NAD cofactor: *nadR*; and phosphorus: *phoU*) (Table S5). Clones lacking genes from either cluster would be at a disadvantage as they would be unable to meet the energy demands of rapid growth, while combating with stress induced by eNM or $ZnCl_2$.

The time-dependent sensitivity of differing biological pathways was also reflected in the time-resolved IC_{50} values of the sensitive clones. Many clones, which were sensitive at early time points in KO screening, showed a marked decrease in absolute toxicity as their respective IC_{50} values increased over time. These clones, which were classified within the mild sensitivity category, represent biological pathways related to ABC transporters and two-component signaling pathways. In contrast, clones detected at later time points, typically membrane-related clones (lipopolysaccharide biosynthesis and cell membrane structure), displayed persistent toxicity (intermediate to high sensitivity), as they exhibited low IC_{50} values that did not increase substantially throughout the 24 h study period. Clones relating to metal homeostasis (metal ion binding and transport) were enriched at both early and late time points and range from high to mild sensitivity. Taken together, the results from the KO screen and time-resolved IC_{50} values suggest that some clones exhibited transient sensitivities during exposure at early time points, while other clones exhibited persistent sensitivities after prolonged exposure. Overall, our time-resolved methodology revealed that different toxicity mechanisms were active at different experimental times, and all of these trends are undetectable with conventional single end-point assays or even single mechanism time-resolved approaches, which are less comprehensive than our full genome-wide scan.

The membrane-related clones (lipopolysaccharide biosynthesis and cell membrane structure) were the largest enriched clusters for all zinc sources, detected as late hits in the initial screen, and maintained a high sensitivity to Zn throughout the 24 h period in IC_{50} analysis. The presence of these clones as sensitive hits suggests the involvement of direct membrane damage or lipid peroxidation, both of which have been observed in Zn-eNM toxicity.[6,12] Exclusion by membrane barriers serves as an important defense against metals entering into the cell.[31] Lipopolysaccharides within the outer membrane have been shown to have an important role in slowing the rate of influx of metals and other toxic compounds into bacterial cells.[32] Furthermore, many efflux pumps are transmembrane proteins; therefore, poor membrane integrity can be expected to hamper their functionality.[33] Our results suggest that clones with membrane deficiencies were unable to recover from toxicity stemming from all

three zinc sources. Moreover, we demonstrate here that end-point assays, which are currently the standard, have a bias toward the detection of injury paradigms, which are related to structural components and lipid biosynthesis (see Figure 4A).

The release of Zn^{2+} into the media and resultant ion damage was an important toxicity mechanism for both zinc eNMs and the $ZnCl_2$ salt as indicated by the enrichment of clusters related to metal homeostasis (metal ion binding and metal ion transport) among all zinc source subgroupings in both the KO screen and IC_{50} analysis. Clones lacking the zinc-specific-ion regulating system of *ZntA* and *ZntR* were the most susceptible to toxicity from Zn-eNMs and $ZnCl_2$ at both time periods and were found to be the most severely growth inhibited during IC_{50} analysis (Table S4: (A) Z-score and (F) IC_{50}). While clusters related to metal homeostasis were present at both time periods, greater enrichment was observed earlier, which may be related to the exponentially growing cells assayed at that time. These results agree with Yamamoto and coworkers who found that, in the presence of excess zinc, *zntA* and other zinc homeostasis genes were rapidly overexpressed during exponential growth of *E. coli* cells.[34] When in excess, Zn^{2+} can compete with other metals such as Ni^{2+}, Co^{2+}, and Fe^{2+} in the biding domain of metalloproteins, and as a result, the incorporation of zinc into nascent polypeptides may be exaggerated in rapidly dividing cells.[35] Therefore, clones with already comprised metalloproteins that fulfill critical functions in the cell will exaggerate this response. Additionally, clones relating to the ABC transporter cluster were enriched during early time points. Of the 18 clones in this cluster, 9 (50%) relate to metal homeostasis (*btuF, entC, fecE, feoA, fepC, nikD, nikA, yebz,* and *zntA*) further linking the combined stress from exponential growth and excess zinc (Table S5).

These shared mechanisms in toxicity pathways may be explained by similar chemical properties observed in each zinc source after exposure to LB. In general, the morphologies and chemical composition of suspended NMs were similar following exposure to the rich organic LB media. Results from the chemical component analysis of powders before and after exposure to LB media highlight that the solution chemistry dominated the dissolution and reprecipitation processes regardless of the form of zinc metal. Zn-containing NMs and salts approached chemical equilibrium in LB media, which is a rich medium with high organic content and ionic strength ($\sim$170 mM). Following partial dissolution, Zn^{2+} ions formed various soluble and solid complexes with media constituents. For example, phosphate complexes comprised the dominant species across all zinc filtrates. Furthermore, the oxide layer formed on nZn suggested by the zeta-potential and EDAX measurements may explain the high percentage of shared hits between nZn and nZnO

in the KO library screen and similar ranges for IC_{50} values. These transformations determined the bioavailable forms of zinc released from each zinc source. The toxicity caused by NMs and salts can be understood as the combined effects of Zn^{2+} and various NMs and NM aggregates, which were not identical to the particles initially added to the media. Furthermore, the exposure of Zn-eNMs and salts in LB mirror the exposure conditions in other waters with high organic content, such as influent at wastewater treatment plants where the accumulation of Zn-eNMs and salts is likely to occur.

In spite of these similarities, free ions alone were not able to explain toxicity as the IC_{50} values of $ZnCl_2$ were generally the lowest and it elicited the most hits in screening relative to either NM. $ZnCl_2$ elicited responses from 70 clones that were not also hits for nZn or nZnO, and at early time points, $ZnCl_2$ showed greater enrichment of clones related to two-component signaling, while nZnO showed greater enrichment of clusters related to monosaccharide biosynthesis. These differences may occur because the bioavailability of zinc may be different when introduced as a free ion ($ZnCl_2$) or as part of an eNM. ICP analysis showed that free Zn^{2+} concentration was similar ($\sim$40 mg/L as Zn^{2+}) for all zinc sources, yet the precipitates of $ZnCl_2$ (17.8 $\pm$ 3.7 nm) were an order of magnitude smaller than either nZn (159 $\pm$ 48 nm) or nZnO (102.2 $\pm$ 22.7 nm). Previous studies of metallic NPs have reported that aggregation can reduce the bioavailability of the metal and resulting toxicity.[36] Aggregation of the particles in the media may have reduced the relative surface area available for reactivity and ion release. This may have resulted in $ZnCl_2$'s differing toxicity behavior and suggests that a more complex model is necessary. In contrast to the free ion activity model, the biotic ligand model, which involves a thorough exploration of solution chemistry and has been shown to be an effective model for predicting zinc toxicity, may be a stronger indicator.[37]

This dichotomy of temporal sensitivities has implications for predictive nanomaterial toxicity assessments. The early toxicity responses, which resulted in temporary growth retardation, were not detectable at later time points, and these transient mechanisms would be ignored using single-point IC_{50} values. This highlights the advantage of our method's ability to distinguish the dynamic time-dependent responses without having any prior knowledge of specific toxicity. This can be contrasted with traditional single time point knowledge-based microarrays or traditional mechanism assays, which reflect isolated responses. Previous toxicity studies, therefore, which have only measured single time points on this collection or utilized similar genome wide methods, may have missed time-sensitive biological responses.[38,39]

Our results suggest that both zinc eNMs as well as salts are toxic due to mechanisms relating to ion

release, membrane damage, and metabolic effects but vary in their timing and severity. Understanding the time dependence of eNM toxicity will be crucial in minimizing the impact of these toxicants to aquatic environments, terrestrial soils, and wastewater treatment plants—the most common sinks for contaminants.[40,41] The first levels of interaction and uptake will be among primary producers, specifically, microorganisms like bacteria. As zinc eNMs have been shown to change the balance and composition of soil bacteria communities, microbes that are better able to rebound against toxicity will grow better and colonize contaminated environments.[42] Previous nanotoxicity studies, for example, have shown that bacteria with more robust Gram-positive membranes have a growth advantage over bacteria with thinner Gram-negative membranes.[43] Differential inhibition, therefore, of microbial communities mediating specific environmental processes can lead to an imbalance between various reservoirs of carbon and nitrogen as well as impact food webs. Recently, researchers found that nZnO severely inhibited the efficiency of phosphorus and nitrogen removal metabolism in anaerobic reactors, suggesting that eNMs entering wastewater streams may impact the efficiency of treatment plants and reduce the ability to treat other contaminants.[44] As the KO library represents varying biological sensitivities observed in mixed communities, this work suggests that zinc eNMs may cause differential shifts in bacterial communities due to differing biological sensitivities. Our results imply that bacteria with sensitive membranes and limited metal efflux will be most affected, while organisms with deficits in their general metabolism may experience more subtle inhibition by zinc eNMs during early growth and colonization. Our results contribute to a better understanding of the toxicity mechanisms induced by exposure to Zn-eNMs, which may be relevant to other metal-containing eNMs such as Cu-eNMs or Fe-eNMs as many metalloproteins can bind to other metals with stronger affinities.[35]

CONCLUSIONS AND PROSPECTS

Here we demonstrate differences in the bacterial response to two types of Zn-eNMs *versus* $ZnCl_2$ bulk material through the utilization of a time-resolved HTS methodology employing an *E. coli* genome-wide knockout library. Through the extensive use of automation, we were able to execute experiments in a matter of days, which would normally take months. Automation was also crucial for acquiring the necessary temporal resolution—which in turn was crucial for capturing a comprehensive view of nano- and bulk toxicity paradigms. At early time points, Zn-eNMs and salts elicited responses related to general metabolic function, transport, signaling, and metal ion homeostasis, while later time points evoked responses from membrane synthesis pathways. The presence of overlapping pathways related to membrane damage and metal ion homeostasis suggests that toxicity is partially related to metal ion release, while the differential sensitivity profiles between nanoscale and bulk material suggest potentially novel nanoscale-specific effects that warrant further examination. For example, at early time points, bulk $ZnCl_2$ elicited responses in pathways related to two-component signaling, while nZnO evoked responses in pathways related to monosaccharide biosynthesis.

The toxicity paradigms in force at early or late time points share little overlap, which emphasizes the need to include time-resolved measurements in all future nanotoxicity studies. We expect that hazard ranking of nanomaterials will become more effective—at least for the widely used zinc-containing nanomaterials examined in this study—as a result of the inclusion of time-resolved data. Furthermore, we expect nanotoxicology assessments to have more predictive power by taking full advantage of this added dimension. The inverse is likely to hold true, as well: It is obvious that single-point measurement driven methodologies—even if they rely on genome wide coverage—will have limited predictive power. For example, a significant portion of the toxicity paradigms in the early phase of the experiments would have been missed with traditional single-point approaches, resulting in an incomplete assessment of the toxicity paradigms for a given eNM. Our future efforts will focus on the elucidation of the differential toxicity modalities that we observed, and we anticipate that high-throughput methodologies will continue to be crucial to the execution of this body of work.

MATERIALS AND METHODS

Nanomaterial Preparation and Characterization. Zinc-containing nanomaterials (Zn-eNMs) were obtained from commercial vendors: nZn (Quantum Sphere, Santa Ana, CA) and nZnO (Meliorum Technologies, Rochester, NY). To assess the contribution of Zn^{2+} ions to observed toxicity, $ZnCl_2$ (>99% purity) was used (Sigma Aldrich, St. Louis, MO). Prior to every assay, fresh zinc stock suspensions (1000 mg/L as zinc) were prepared by mixing Zn-eNMs and $ZnCl_2$ salt into Luria—Bertani (LB) broth media, followed by sonication in an ultrasonic bath for 30 min at maximum power (FS30H, Fisher Scientific, 100 W, 42 kHz). All stocks were sonicated

1 min before use and diluted to their final concentration using LB within 3 h of preparation of the stock solution.

To determine particle size and zeta-potentials in solution, a final concentration of 100 mg/L as Zn^{2+}, Zn-eNMs/LB solutions were incubated at 37 °C, and measurements were taken every 6 h over a 24 h period. The hydrodynamic diameters (aggregate sizes) of Zn-eNMs were determined in LB media by dynamic light scattering (BI 90Plus, Brookhaven Instruments Corp., Holtsville, NY), and zeta-potentials (mobility) were computed from measured electrophoretic motilities (ZetaPALS, Brookhaven Instruments Corp).

Dissolved zinc concentrations were measured by inductively coupled plasma optical emission spectroscopy (ICP-OES) according to U.S. EPA 3050B standard method. In brief, Zn-eNMs and $ZnCl_2$/LB media solutions (100 mg/L as Zn^{2+}) were incubated at 37 °C for 24 h, then centrifuged and filtered through 3 kDa ultrafiltration membranes (Amicon Ultra-4 3K, Millipore, Billerica, MA) for 30 min at 2800g. The filtrate was digested in HNO_3 followed by ICP-OES measurements.

The NMs' morphologies and chemical compositions were analyzed by field-emission scanning electron microscopy (FESEM; JEOL, JSM-6700F) equipped with an EDAX system (Genesis, EDAX). The particles were examined prior to and after introducing into LB media. As-received nZn and nZnO nanomaterials examined in dry power form served as a baseline for comparison. Additionally, the solid particles in LB media, consisting of insoluble NMs and precipitates formed by excess Zn^{2+} ion complexation with LB constituents, were collected after 24 h incubation at 37 °C, using 0.03 μm polycarbonate track etch membranes (Sterlitech, WA) and dried in vacuum desiccators. Image analysis software, Image Pro (MediaCybernetics), was used to determine the particles' sizes. The chemical compositions of the solid particles collected were determined by EDAX analysis.

E. coli Cells and Knockout (KO) Library. The Keio library comprises 3985 single knockout *E. coli* clones which encompasses about 90% (4390 total genes) of the genome of the base strain, BW25113.[26] Each KO clone carries a deletion of a single gene, with a kanamycin resistance gene serving as the replacement. The library was maintained in 12 384-well clear microtiter plates (Greiner Bio-One, Monroe, NC) in 10% glycerol/LB broth containing 25 μg/mL of kanamycin and stored at -80 °C. BW25113 was used as the control wild-type (wt) strain for each experiment and was cultured identically as the library, but was grown in LB in the absence of kanamycin. Prior to running toxicity assays, frozen microtiter stocks were precultured in fresh LB media at 37 °C for 24 h before being transferred to LB without kanamycin. The Q-bot replicator (Genetix, New Milton, England) was used to pin a microdrop of cells between 384-well plates to transfer cells.

Wild-Type IC_{50}. The wt strain was exposed to a dilution series of each zinc source to determine an appropriate concentration for the KO library screen. Briefly, wt cells from precultured microtiter plates were pinned into 384-well plates containing 80 μL of fresh LB media with Zn-eNMs and salts at final concentrations ranging from 0.2 μg/L to 500 mg/L as Zn^{2+} (2-fold dilutions between each concentration). Each condition was tested with at least eight replicates. Clones were incubated for 24 h at 37 °C, and growth was measured by transmittance (OD_{600nm}) every 2 h using the Acquest plate reader (Molecular Devices). Growth was assayed every 2 h to capture the lag, exponential, and stationary growth phases. Wells containing only *E. coli* cells (no added zinc) or Zn-eNMs and $ZnCl_2$ (abiotic) served as controls. Absorbance data were fitted using a nonlinear regression dose response model employing a four-parameter logistic equation (Prism 4, GraphPad Software, San Diego, CA), which was used to calculate the IC_{50} values and 95% confidence intervals (see Table 1 for results). IC_{50} values were determined for every 2 h time point after 6 h.

KO Screening. To determine the most sensitive clones, the library was screened against the 24 h IC_{50} concentration obtained in the initial wt screen (Table 1). After preculturing, the cells from the library were pinned into 384-well plates containing 80 μL of LB at the appropriate IC_{50} concentration. For comparison, cells from the library were also pinned into 80 μL of LB with no added zinc. All conditions were run in triplicate to account for biological, systematic, plate-to-plate, and run-to-run variability. Plates were incubated at 37 °C for a 24 h period, and transmittance (OD_{600nm}) was measured every 6 h using the Acquest plate reader (Molecular devices). As readings were taken every 6 h, measurements reflect growth at lag, exponential, and stationary phases of *E. coli* growth. A total of 221 184 readings were processed for KO screening (12 library plates × 3 replicates × (3 zinc sources + 1 control) × 384 wells × 4 time points).

Data Normalization and Hit Selection. Data normalization occurred in two steps. First, to account for growth differences

TABLE 1. IC_{50} Values for the Wild-Type *E. coli* after Exposure to $ZnCl_2$, nZn, and $nZnO$[a]

time (h)		IC_{50} (mg/L as Zn^{2+})	
	$ZnCl_2$	nZn	nZnO
6	40.8 ± 13.6	96.4 ± 7.5	68.4 ± 6.6
8	40.8 ± 25.1	110.3 ± 4.9	86.6 ± 6.2
10	40.6 ± 29.6	113.2 ± 4.7	92.5 ± 4.8
12	47.6 ± 4.6	114.1 ± 4.0	95.1 ± 4.0
14	54.0 ± 4.5	117.9 ± 4.1	99.1 ± 3.5
16	59.3 ± 4.6	121.1 ± 3.6	102.2 ± 3.3
18	63.8 ± 4.5	124.9 ± 2.9	106.5 ± 3.0
20	68.7 ± 4.4	127.5 ± 2.1	110.7 ± 3.4
22	71.1 ± 4.2	131.6 ± 2.5	115.2 ± 3.5
24	73.7 ± 4.2	131.6 ± 2.1	119.3 ± 2.9

[a] With respect to the zinc source, the toxicity decreased with the following trend: $ZnCl_2$ > nZnO > nZn. For all sources, toxicity decreased with time. Errors represent 95% CI interval.

between control and experimental cells, the $\log_2$ average transmittance of the clone exposed to the IC_{50} concentration was divided by the $\log_2$ average transmittance from the unexposed control. Since lower bacterial growth resulted in higher measured transmittance, larger ratios of exposed to unexposed cells indicated more sensitive clones. Next, the robust Z-score method using the median absolute deviation (MAD) method was employed to determine which clones had a statistically significant difference in growth relative to the entire library.[27] The robust Z-score was computed according to the following equation:

$$MAD = 1.4826 \times median(|X_{ij} - median(X_j)|)$$

$$Robust\ Z = (X_{ij} - median(X_j))/MAD$$

where X_{ij} is the ratio of the transmittance of the exposed control to the unexposed control for well i in plate j and median (X_j) is the median of the ratios in plate j. For each clone, the average robust Z-score was calculated for significance testing. Z-score methods were used to transform data so that it reflected a normal distribution, where scores are indicative of the distance from the central values. In order to find more sensitive clones, a clone was considered a hit when its Z-score was greater than 2.5 at any of the 4 time points (6, 12, 18, and 24 h), which represents outliers comprising less than 0.5% of the theoretical normal distribution.[28] Unlike traditional Z-score methods, using the MAD and median as indicators of distribution and central tendency, respectively, protects these estimates from outliers, which can skew estimations of the distribution and hide significant hits.[45] Hierarchical clustering analysis (HCA) was used to compare the relatedness of the Z-scores of each treatment. In HCA analysis, the distance metric was set as Euclidean distance and the linkage method was set as Ward's linkage clustering.[46]

IC_{50} Values for Selected Clones. In order to characterize the different sensitivities of each clone identified as a hit, the selected clones were exposed to a dilution series of each zinc source to calculate IC_{50} values (Figure 1B). Using the Q-bot, sensitive clones identified in the KO screen were rearrayed from the original library into a single 384-well clear plate. After preculturing, the cells were pinned into a series of microtiter plates containing LB/zinc suspensions at 10 different concentrations. Each dilution series was based around the IC_{50} value of the respective metal source (three 2-fold dilutions above and seven 2-fold dilutions below). Each concentration was run in triplicate, plates were incubated for 24 h at 37 °C, and transmittance (OD_{600nm}) readings were taken at 8 and 22 h. The IC_{50} values were calculated for each time point using the same nonlinear regression model used for the wt. A total of 69 120

readings were processed for assessing IC_{50} values (10 plate dilution series × 3 zinc sources × 3 replicates × 384 wells × 2 time points). HCA was used to compare the relatedness of the IC_{50} values of each treatment, and HCA was performed as previously highlighted for Z-scores.

Gene Annotation and Cluster Enrichment. The Database for Annotation, Visualization and Integrated Discovery (DAVID) v6.7, National Institute of Allergy and Infectious Diseases (NIAID), National Instituted of Health (NIH), was used to annotate the gene lists obtained from the KO library and enrich for sensitive clusters.[29] This Internet-based resource integrates multiple databases such as GO, KEGG Pathways, and BioCarta to rapidly analyze gene lists from high-throughput data and assign biological meaning. DAVID's functional annotation clustering algorithm employs fuzzy heuristic clustering to determine the overrepresentation of related biological annotation terms relative to their representation in the reference genome. Clusters with a combined p value greater than 0.05 were considered significant.

Conflict of Interest: The authors declare no competing financial interest.

Supporting Information Available: Zeta-potential, aggregate particle size, chemical composition of zinc nanomaterials and salts, and heat maps of clone IC_{50} values were analyzed. Tables of clone descriptions, Z-scores, library screen hit patterns, clustering, and individual clone IC_{50} values are also described. This material is available free of charge *via* the Internet at http://pubs.acs.org.

REFERENCES AND NOTES

1. George, S.; Xia, T.; Rallo, R.; Zhao, Y.; Ji, Z.; Lin, S.; Wang, X.; Zhang, H.; France, B.; Schoenfeld, D.; *et al.* Use of a High-Throughput Screening Approach Coupled with *In Vivo* Zebrafish Embryo Screening To Develop Hazard Ranking for Engineered Nanomaterials. *ACS Nano* **2011**, *5*, 1805–1817.

2. Jiang, W.; Mashayekhi, H.; Xing, B. S. Bacterial Toxicity Comparison between Nano- and Micro-Scaled Oxide Particles. *Environ. Pollut.* **2009**, *157*, 1619–1625.

3. Adams, L. K.; Lyon, D. Y.; Alvarez, P. J. J. Comparative Eco-Toxicity of Nanoscale TiO_2, SiO_2, and ZnO Water Suspensions. *Water Res.* **2006**, *40*, 3527–3532.

4. Lee, C. W.; Mahendra, S.; Zodrow, K.; Li, D.; Tsai, Y.-C.; Braam, J.; Alvarez, P. J. J. Developmental Phytotoxicity of Metal Oxide Nanoparticles to *Arabidopsis thaliana*. *Environ. Toxicol. Chem.* **2010**, *29*, 669–675.

5. Li, Q.; Mahendra, S.; Lyon, D. Y.; Brunet, L.; Liga, M. V.; Li, D.; Alvarez, P. J. J. Antimicrobial Nanomaterials for Water Disinfection and Microbial Control: Potential Applications and Implications. *Water Res.* **2008**, *42*, 4591–4602.

6. Premanathan, M.; Karthikeyan, K.; Jeyasubramanian, K.; Manivannan, G. Selective Toxicity of ZnO Nanoparticles toward Gram-Positive Bacteria and Cancer Cells by Apoptosis through Lipid Peroxidation. *Nanomedicine* **2011**, *7*, 184–192.

7. Hanley, C.; Layne, J.; Punnoose, A.; Reddy, K. M.; Coombs, I.; Coombs, A.; Feris, K.; Wingett, D. Preferential Killing of Cancer Cells and Activated Human T Cells Using ZnO Nanoparticles. *Nanotechnology* **2008**, *19*, 10.

8. Thomas, C. R.; George, S.; Horst, A. M.; Ji, Z. X.; Miller, R. J.; Peralta-Videa, J. R.; Xia, T. A.; Pokhrel, S.; Madler, L.; Gardea-Torresdey, J. L.; *et al.* Nanomaterials in the Environment: From Materials to High-Throughput Screening to Organisms. *ACS Nano* **2011**, *5*, 13–20.

9. Som, C.; Berges, M.; Chaudhry, Q.; Dusinska, M.; Fernandes, T. F.; Olsen, S. I.; Nowack, B. The Importance of Life Cycle Concepts for the Development of Safe Nanoproducts. *Toxicology* **2010**, *269*, 160–169.

10. Li, M.; Zhu, L.; Lin, D. Toxicity of ZnO Nanoparticles to *Escherichia coli*: Mechanism and the Influence of Medium Components. *Environ. Sci. Technol.* **2011**, *45*, 1977–1983.

11. Bai, W.; Zhang, Z.; Tian, W.; He, X.; Ma, Y.; Zhao, Y.; Chai, Z. Toxicity of Zinc Oxide Nanoparticles to Zebrafish Embryo: A Physicochemical Study of Toxicity Mechanism. *J. Nanopart. Res.* **2011**, *12*, 1645–1654.

12. Zhang, L. L.; Jiang, Y. H.; Ding, Y. L.; Daskalakis, N.; Jeuken, L.; Povey, M.; O'Neill, A. J.; York, D. W. Mechanistic Investigation into Antibacterial Behaviour of Suspensions of ZnO Nanoparticles against *E. coli*. *J. Nanopart. Res.* **2010**, *12*, 1625–1636.

13. Zhang, H. Y.; Ji, Z. X.; Xia, T.; Meng, H.; Low-Kam, C.; Liu, R.; Pokhrel, S.; Lin, S. J.; Wang, X.; Liao, Y. P.; *et al.* Use of Metal Oxide Nanoparticle Band Gap To Develop a Predictive Paradigm for Oxidative Stress and Acute Pulmonary Inflammation. *ACS Nano* **2012**, *6*, 4349–4368.

14. Rallo, R.; France, B.; Liu, R.; Nair, S.; George, S.; Damoiseaux, R.; Giralt, F.; Nel, A.; Bradley, K.; Cohen, Y. Self-Organizing Map Analysis of Toxicity-Related Cell Signaling Pathways for Metal and Metal Oxide Nanoparticles. *Environ. Sci. Technol.* **2011**, *45*, 1695–1702.

15. George, S.; Pokhrel, S.; Xia, T.; Gilbert, B.; Ji, Z.; Schowalter, M.; Rosenauer, A.; Damoiseaux, R.; Bradley, K. A.; Mädler, L.; *et al.* Use of a Rapid Cytotoxicity Screening Approach To Engineer a Safer Zinc Oxide Nanoparticle through Iron Doping. *ACS Nano* **2009**, *4*, 15–29.

16. Lin, W. S.; Xu, Y.; Huang, C. C.; Ma, Y. F.; Shannon, K. B.; Chen, D. R.; Huang, Y. W. Toxicity of Nano- and Micro-Sized ZnO Particles in Human Lung Epithelial Cells. *J. Nanopart. Res.* **2009**, *11*, 25–39.

17. Li, M.; Pokhrel, S.; Jin, X.; Mädler, L.; Damoiseaux, R.; Hoek, E. M. V. Stability, Bioavailability, and Bacterial Toxicity of ZnO and Iron-Doped ZnO Nanoparticles in Aquatic Media. *Environ. Sci. Technol.* **2010**, *45*, 755–761.

18. Ivask, A.; Suarez, E.; Patel, T.; Boren, D.; Ji, Z.; Holden, P.; Telesca, D.; Damoiseaux, R.; Bradley, K. A.; Godwin, H. Genome-Wide Bacterial Toxicity Screening Uncovers the Mechanisms of Toxicity of a Cationic Polystyrene Nanomaterial. *Environ. Sci. Technol.* **2012**, *46*, 2398–2405.

19. Kim, I. K.; Lee, S. H.; Kim, Y. R.; Seo, S. H.; Jeong, S. H.; Son, S. W.; Kim, M. K. Profiling of Gene Expression in Human Keratinocyte Cell Line Exposed to Quantum Dot Nanoparticles. *Mol. Cell. Toxicol.* **2009**, *5*, 51–57.

20. Poynton, H. C.; Lazorchak, J. M.; Impellitteri, C. A.; Smith, M. E.; Rogers, K.; Patra, M.; Hammer, K. A.; Allen, H. J.; Vulpe, C. D. Differential Gene Expression in *Daphnia magna* Suggests Distinct Modes of Action and Bioavailability for ZnO Nanoparticles and Zn Ions. *Environ. Sci. Technol.* **2010**, *45*, 762–768.

21. Michiels, S.; Kramar, A.; Koscielny, S. Multidimensionality of Microarrays: Statistical Challenges and (Im)Possible Solutions. *Mol. Oncol.* **2011**, *5*, 190–196.

22. Aardema, M. J.; MacGregor, J. T. Toxicology and Genetic Toxicology in the New Era of "Toxicogenomics": Impact of "-Omics" Technologies. *Mutat. Res., Fundam. Mol. Mech. Mutagen.* **2002**, *499*, 13–25.

23. Damoiseaux, R.; George, S.; Li, M.; Pokhrel, S.; Ji, Z.; France, B.; Xia, T.; Suarez, E.; Rallo, R.; Madler, L.; *et al.* No Time To Lose—High Throughput Screening To Assess Nanomaterial Safety. *Nanoscale* **2011**, *3*, 1345–1360.

24. Nel, A. E.; Madler, L.; Velegol, D.; Xia, T.; Hoek, E. M. V.; Somasundaran, P.; Klaessig, F.; Castranova, V.; Thompson, M. Understanding Biophysicochemical Interactions at the Nano-Bio Interface. *Nat. Mater.* **2009**, *8*, 543–557.

25. Gou, N.; Onnis-Hayden, A.; Gu, A. Z. Mechanistic Toxicity Assessment of Nanomaterials by Whole-Cell-Array Stress Genes Expression Analysis. *Environ. Sci. Technol.* **2010**, *44*, 5964–5970.

26. Baba, T.; Ara, T.; Hasegawa, M.; Takai, Y.; Okumura, Y.; Baba, M.; Datsenko, K. A.; Tomita, M.; Wanner, B. L.; Mori, H. Construction of *Escherichia coli* K-12 in-Frame, Single-Gene Knockout Mutants: The Keio Collection. *Mol. Syst. Biol.* **2006**, 2.

27. Chung, N.; Zhang, X. D.; Kreamer, A.; Locco, L.; Kuan, P.-F.; Bartz, S.; Linsley, P. S.; Ferrer, M.; Strulovici, B. Median Absolute Deviation To Improve Hit Selection for Genome-Scale RNAi Screens. *J. Biomol. Screening* **2008**, *13*, 149–158.

28. Zhang, X. D. Illustration of Ssmd, Z Score, Ssmd*, Z* Score, and T Statistic for Hit Selection in Rnai High-Throughput Screens. *J. Biomol. Screening* **2011**, *16*, 775–785.

29. Huang, D. W.; Sherman, B. T.; Lempicki, R. A. Systematic and Integrative Analysis of Large Gene Lists Using David Bioinformatics Resources. *Nat. Protoc.* **2008**, *4*, 44–57.

30. lvarez, O. A.; Jager, T.; Colao, B. N.; Kammenga, J. E. Temporal Dynamics of Effect Concentrations. *Environ. Sci. Technol.* **2006**, *40*, 2478–2484.

31. Choudhury, R.; Srivastava, S. Zinc Resistance Mechanisms in Bacteria. *Curr. Sci.* **2001**, 81.

32. Nishino, K.; Hsu, F. F.; Turk, J.; Cromie, M. J.; Wosten, M.; Groisman, E. A. Identification of the Lipopolysaccharide Modifications Controlled by the Salmonella PmrA/PmrB System Mediating Resistance to Fe(III) and Al(III). *Mol. Microbiol.* **2006**, *61*, 645–654.

33. Nies, D. H. Efflux-Mediated Heavy Metal Resistance in Prokaryotes. *FEMS Microbiol. Rev.* **2003**, *27*, 313–339.

34. Yamamoto, K.; Ishihama, A. Transcriptional Response of *Escherichia coli* to External Zinc. *J. Bacteriol.* **2005**, *187*, 6333–6340.

35. Waldron, K. J.; Robinson, N. J. How Do Bacterial Cells Ensure That Metalloproteins Get the Correct Metal? *Nat. Rev. Microbiol.* **2009**, *7*, 25–35.

36. Albanese, A.; Chan, W. C. W. Effect of Gold Nanoparticle Aggregation on Cell Uptake and Toxicity. *ACS Nano* **2011**, *5*, 5478–5489.

37. Clifford, M.; McGeer, J. C. Development of a Biotic Ligand Model for the Acute Toxicity of Zinc to *Daphnia pulex* in Soft Waters. *Aquat. Toxicol.* **2009**, *91*, 26–32.

38. Liu, A.; Tran, L.; Becket, E.; Lee, K.; Chinn, L.; Park, E.; Tran, K.; Miller, J. H. Antibiotic Sensitivity Profiles Determined with an *Escherichia coli* Gene Knockout Collection: Generating an Antibiotic Bar Code. *Antimicrob. Agents Chemother.* **2010**, *54*, 1393–1403.

39. Tamae, C.; Liu, A.; Kim, K.; Sitz, D.; Hong, J.; Becket, E.; Bui, A.; Solaimani, P.; Tran, K. P.; Yang, H.; *et al.* Determination of Antibiotic Hypersensitivity among 4,000 Single-Gene-Knockout Mutants of *Escherichia coli*. *J. Bacteriol.* **2008**, *190*, 5981–5988.

40. Scown, T. M.; van Aerle, R.; Tyler, C. R. Review: Do Engineered Nanoparticles Pose a Significant Threat to the Aquatic Environment? *Crit. Rev. Toxicol.* **2010**, *40*, 653–670.

41. Klaine, S. J.; Alvarez, P. J. J.; Batley, G. E.; Fernandes, T. F.; Handy, R. D.; Lyon, D. Y.; Mahendra, S.; McLaughlin, M. J.; Lead, J. R. Nanomaterials in the Environment: Behavior, Fate, Bioavailability, and Effects. *Environ. Toxicol. Chem.* **2008**, *27*, 1825–1851.

42. Ge, Y. G.; Schimel, J. P.; Holden, P. A. Evidence for Negative Effects of TiO_2 and ZnO Nanoparticles on Soil Bacterial Communities. *Environ. Sci. Technol.* **2012**, *45*, 1659–1664.

43. Sinha, R.; Karan, R.; Sinha, A.; Khare, S. K. Interaction and Nanotoxic Effect of ZnO and Ag Nanoparticles on Mesophilic and Halophilic Bacterial Cells. *Bioresour. Technol.* **2011**, *102*, 1516–1520.

44. Zheng, X.; Wu, R.; Chen, Y. Effects of ZnO Nanoparticles on Wastewater Biological Nitrogen and Phosphorus Removal. *Environ. Sci. Technol.* **2011**, *45*, 2826–2832.

45. Birmingham, A.; Selfors, L. M.; Forster, T.; Wrobel, D.; Kennedy, C. J.; Shanks, E.; Santoyo-Lopez, J.; Dunican, D. J.; Long, A.; Kelleher, D.; *et al.* Statistical Methods for Analysis of High-Throughput RNA Interference Screens. *Nat. Methods* **2009**, *6*, 569–575.

46. Andreopoulos, B.; An, A. J.; Wang, X. G.; Schroeder, M. A Roadmap of Clustering Algorithms: Finding a Match for a Biomedical Application. *Briefings Bioinf.* **2009**, *10*, 297–314.